ISSN 0912-232X

PHOTOMEDICINE AND PHOTOBIOLOGY

Vol.41 2019

The Japanese Society for Photomedicine and Photobiology

Photomedicine and Photobiology
Vol.41

2019

The Japanese Society for Photomedicine and Photobiology
Foundednin 1978

Office : Depaetment of Dermatology, Kobe University Graduate School of Medicine,
7-5-1 Kusunoki-cho, Chuo-ku, Kobe, 650-0017, Japan.

CONTENTS

Chlorophyll *f* was found as a minor pigment in a unicellular cyanobacterium, strain KC1, isolated from Lake Biwa, cultivated under incandescent light

Chihiro Tanimoto[1], Akihiro Nagashima[2], Tomoya Katsuno[1], Tomohito Mayumi[1], Kotaro Kobayashi[3], Iwane Suzuki[3], Hideaki Miyashita[2,4], and Masami Kobayashi[1*]

[1] *Department of Materials Science, Faculty of Pure and Applied Sciences, University of Tsukuba, Ibaraki 350-8573, Japan*
[2] *Graduate School of Human and Environmental Studies, Kyoto University, Kyoto, 606-8501, Japan*
[3] *Faculty of Life and Environmental Sciences, University of Tsukuba, Ibaraki 305-8572, Japan*
[4] *Graduate School of Global and Environmental Studies, Kyoto University, Kyoto 606-8501, Japan*

***Corresponding author:**

Department of Materials Science, Faculty of Pure and Applied Sciences, University of Tsukuba, Ibaraki 350-8573, Japan
TEL: +81-298-53-6940
FAX: +81-298-53-4490
E-mail: masami@ims.tsukuba.ac.jp

ABSTRACT

Previously chlorophyll *f* was found as a minor pigment in a unicellular cyanobacterium, strain KC1 isolated from Lake Biwa, when cultivated under far-red LED light, whereas Chl *f* was not observed at all under white fluorescent light. A very small amount of Chl *f* was detected for the first time in strain KC1 grown under incandescent light.

Key words: chlorophyll *a*, chlorophyll *d*, chlorophyll *f*, KC1

Abbreviations: Car-carotenoid; Chl-chlorophyll; HPLC-high performance liquid chromatography; PS-photosystem

Introduction

A red-shifted chlorophyll, Chl *f* (Fig. 1), was first found in a methanolic extract of cells predominating in the enrichment culture of microalgae collected from Shark Bay stromatolites.[1] Shortly afterward, a cyanobacterium producing Chl *f* only when cultivated under far-red light (FR light) was discovered there, and was then named *Halomicronema hongdechloris*.[2] At around the same time, a Chl *f*-producing unicellular cyanobacterium, strain KC1, was isolated from freshwater environment, Lake Biwa, while Chl *f* was also detected only when cultivated under FR light.[3, 4, 5] The amount of Chl *f* in these algae grown under FR light was very small, and its function has not been clarified to date.

As shown in Fig. 2, there is slight but significant overlap between emission spectrum of FR LED light and absorption spectrum of the strain KC1 cells cultivated under FR LED light, where a small absorption shoulder around 700 nm derived from Chl *f* in the cells overlaps with the foot of emission spectrum of FR LED light, arising from acclimation to FR LED light. However, such a shoulder cannot be seen in the cells grown under white fluorescent light, and no production of Chl *f* takes place.

It is of interest to note that incandescent light can be absorbed by the small absorption shoulder derived from Chl *f* (Fig. 2), and hence Chl *f* is expected to be found also in the KC1 cells cultivated even under incandescent light. In this paper, we investigate whether Chl *f* is observed in the strain KC1 cells grown under incandescent light.

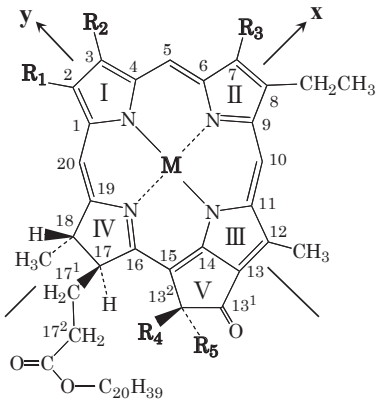

	M	R_1	R_2	R_3	R_4	R_5
Chl *a*	Mg	CH_3	$CH{=}CH_2$	CH_3	H	$COOCH_3$
Chl *b*	Mg	CH_3	$CH{=}CH_2$	CHO	H	$COOCH_3$
Chl *d*	Mg	CH_3	CHO	CH_3	H	$COOCH_3$
Chl *f*	Mg	CHO	$CH{=}CH_2$	CH_3	H	$COOCH_3$
Chl *a'*	Mg	CH_3	$CH{=}CH_2$	CH_3	$COOCH_3$	H
Phe *a*	2H	CH_3	$CH{=}CH_2$	CH_3	H	$COOCH_3$

Fig. 1 Molecular structures of Chls *a*, *b*, *d*, *f*, *a*' and Phe *a* according to the IUPAC numbering system.

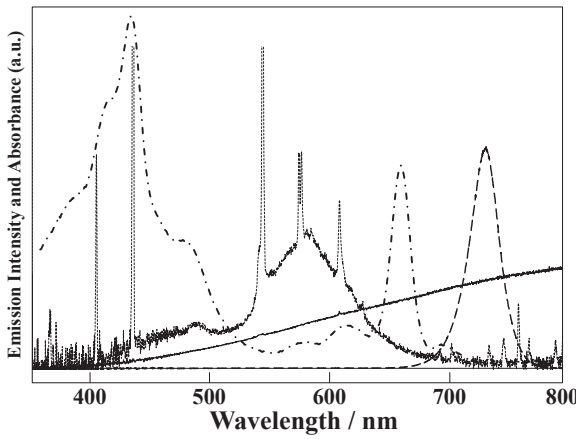

Fig. 2 Emission spectra of white fluorescent light (·····), incandescent light (——), FR LED light (−−−), and absorption spectrum in acetone for acetone/methanol extracts of the strain KC1 cells grown under FR LED light (−·−·−).

Materials and Methods

Algal culture

Cells of the strain KC1 cyanobacterium were grown in BG-11 medium in a glass cell culture flask (1 L) at 297 K with continuous air-bubbling. Cells were incubated under continuous white fluorescent light (TOSHIBA, FL6W, 50 μmol photons/m^2/s), incandescent bulb (National, Silica 100V90W, 20 μmol photons/m^2/s) or far-red LED light (SANYO, MIL-18(A), 740 nm peak, 30 μmol photons/m^2/s). Cells at the early stationary phase were harvested by centrifugation. The cell pellet was stored in a refrigerator at 193 K until use.

Pigment preparation

Chlorophyll *f* was extracted with acetone/methanol (7/3, *v*/*v*) mixture at 277 K from the Chl *f*-containing cyanobacterium strain KC1 grown under FR-LED light. The extract was applied to a preparative-scale HPLC (Senshu Pak 5251-N, 250 mm x 20 mm i.d.) and eluted with hexane/ 2-propanol/methanol (100/2/0.4, *v*/*v*/*v*) at a flow rate of 7 mL min^{-1} at 277 K, as described elsewhere. [6] Chlorophylls *a* and *b* were extracted from parsley (*Petroselinum crispum* Nym.), which were then purified by the same method as for Chl *f*. Other authentic pigments, Chl *a'* and Phe *a*, were prepared by epimerization and pheophytinization of Chl *a* as described elsewhere.[7]

Pigment analysis

Pigments were extracted from cell suspension (ca. 10 μL) by sonication in a ca. 300-fold volume of acetone/methanol (7/3, *v*/*v*) mixture for 2 min in the dark at ca. 277 K. The extract was filtered and dried *in vacuo*. The whole procedure was completed within 5 min. The solid material thus obtained was immediately dissolved in ca. 10 μL of chloroform, and injected into a silica HPLC column (YMC-Pak SIL, 250 x 4.6 mm i.d.) cooled to 277 K in an ice-water bath. The pigments were eluted isocratically with degassed hexane/2-propanol/methanol (100/1/0.4, *v*/*v*/*v*) at a flow rate of 1.0 mL min^{-1}, and were monitored with a JASCO UV-1570 detector (λ = 404 nm) and a JASCO photodiode array detector MD-915 (λ = 300 - 800 nm) in series. The pigments remaining in the flask was dissolved in acetone, and its absorption spectrum was measured with a JASCO V-560.

The Chl *f* /*a'* and Chl *f* /Phe *a* ratios were calculated from the corresponding HPLC peak area ratios by assuming that the $Q_{Y(max)}$ molar extinction coefficient of Chl *f* is the same as that of Chl *d*.[8]

Results and discussion

The absorption spectra in acetone for pigment extracts from the strain KC 1 cells cultivated under white fluorescent light, incandescent light or far-red LED light are shown in Fig. 3. Contrary to our expectations, the corresponding shoulder peak around 700 nm brought about by Chl *f* is hardly observed in the spectrum for pigment extracts from strain KC1 cells cultivated under incandescent light, which intimate to us that Chl *f* might be absent from the KC1 cells grown under incandescent light.

We, however, noted that the strain KC1 cells cultivated under FR light contained ca. 8 Chl *f* molecules per 100Chls *a* (Fig. 4C), which made a small shoulder around 700 nm being capable of finding Chl *f* even by the simple absorption spectrum method (Fig. 2). If Chl *f* was far too little, e.g. 1-2Chls *f*/100Chls *a*, to make such a characteristic absorption shoulder, one would not be able to notice Chl *f* exiting from the absorption spectrum.

In such a case, however, HPLC with high sensitivity is able to detect Chl *f* even below the level of one Chl *f*

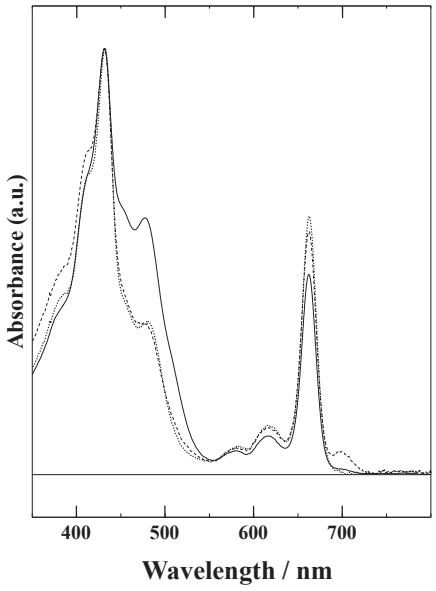

Fig. 3 Absorption spectra in acetone for acetone/methanol extracts of cells of strain KC1 acclimated under the different light conditions; white fluorescent light (·····), incandescent light (——) and FR-LED light (−−−). Absorption spectra are normalized by the Soret peaks.

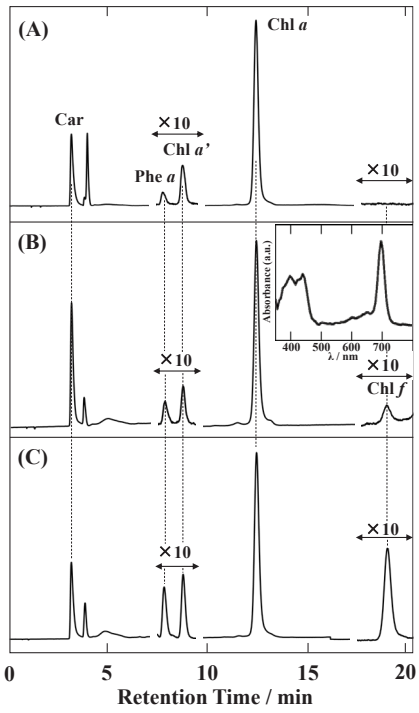

Fig. 4 Normal-phase HPLC elution profiles for acetone/methanol extracts of cells of strain KC1 cultivated under (A) white fluorescent light, (B) incandescent light and (C) FR-LED light. The pigments were eluted isocratically with a degassed solvent mixture of hexane/2-propanol/methanol (100/1/0.4) at a flow rate of 1.0 mL min^{-1} at 277 K, monitored with a monochromator at the wavelength of 404 nm, and recorded with Rec-PRO, Runtime Instruments. Absorption spectrum of Chl *f* detected on the chromatogram (B) was measured by the photodiode array detector, and is inset into the chromatogram. The peak after Car comes from the injection solvent.

molecule per 100Chls *a*. Typical HPLC traces for acetone/methanol extracts from cells of the cyanobacterium strain KC1 grown under white fluorescent light, incandescent light and FR LED light (λ_{max} = 740 nm) are shown in Fig. 4. A large amount of Chl *a*, as well as small amounts of Chl *a'* and Phe *a*, were detected without exceptions. In addition, the strain KC1 grown under FR LED light showed the presence of Chl *f* as a minor pigment (Fig. 4C), but a complete absence of Chl *f* under white fluorescent light (Fig. 4A) as reported previously.[9] As had been expected, for the first time Chl *f* was found when cultivated under incandescent light, while the amount was infinitesimally small (Fig. 4B). The corresponding peak showed the absorption spectrum characteristic of Chl *f* (see inset).

The molar ratio of Chl *f*/100Chl *a* in the cells of the strain KC1 grown under incandescent light is found to be 1.6, while the corresponding ratio under FR LED light is considerably larger, ca. 8.2. Under incandescent light, pigment stoichiometries of Chl *f*/Chl *a'* and Chl *f*/Phe *a* are 1.1 and 2.2, respectively. On the basis of Chl *a'*/PS I = 1/1 and Phe *a*/PS II = 2/1,[10] stoichiometries of Chl *f*/PS I and Chl *f*/PS II in the cells grown under incandescent light are calculated to be ca. 1 and 4, respectively, revealing Chl *f* to be present in either only PS I or only PS II. At the moment we cannot say which photosystem contains Chl *f* under incandescent light.

According to our previous study, however, stoichiometries of PS I/PS II (= Chl *a'*/2Phe *a*) changed from 6.5 under white fluorescent light to 2.7 under FR LED light,[9] and similar tendency was observed in the present study (see Figs. 4A and C). The PS I/PS II stoichiometry in the cells grown under incandescent light examined here is 4.1, which is intermediate between them. Taking into account such acclimation to light, we have assumed that Chl *f* might exist only in PS II in the strain KC1 cells grown under incandescent light, which is supported in part by the recent study on PS I and PS II preparations isolated from the cells grown under FR light showing Chl *f*/PS I = 7-8 and Chl *f*/PS II = 4.[11] However, in order to confirm our expectations, further studies, *e.g.* precise pigment analyses of PS I and PS II preparations from cells grown under incandescent light, are eagerly awaited, and such experiments are now under way.

Further, there remains a possibility that Chl *f* might be generated in the inner cells of a glass cell culture flask. Due to the light shielding effect of the surrounding cells, the inner cells may be considerably exposed to the light in the FR region from light bulbs. In order to exclude the light shielding effect, it is necessary to culture the cells in a thin culture container, and the attempt is also ongoing,

We should pay close attention to carotenoids as well as chlorophylls, since when turning our eyes to the absorption spectra of pigment extracts in the 450 nm to 500 nm region, the cells grown under incandescent light shows a marked difference, namely, the higher ratio of carotenoids/Chls under incandescent light (Fig. 3). The result suggests Chl *f* to be inducted by not only self-shading effects but also acclimation to incandescent light. At present, however, it is vague why the Cars/Chls ratio is higher under incandescent light and where extraneous carotenoids are located in the cells grown under incandescent light, and hence studies of Car are also needed.

References

1. Chen M, Schliep M, Willows RD, Cai Z, Neilan BA, Scheer H. A red-shifted chlorophyll. Science, 2010; 329: 1318-1319.
2. Chen M, Li Y, Birch D, Willows RD. A cyanobacterium that contains chlorophyll *f* – a red-absorbing photopigment. FEBS Lett, 2012; 586: 3249-3254.
3. Ohkubo S, Usui H, Miyashita H. Unique chromatic adaptation of a unicellular cyanobacterium newly isolated from Lake Biwa. Jpn J Phycol (Sorui), 2011; 59: 52(A22) (in Japanese).
4. Kobayashi M**,** Akutsu S, Fujinuma D, et al. Physicochemical Properties of Chlorophylls in Oxygenic Photosynthesis–Succession of co-factors from anoxygenic to oxygenic photosynthesis. In:

Dubinsky Z, ed. Photosynthesis, Croatia, Intech, 2013: Chapter 3, 47-90.
5. Miyashita H, Ohkubo S, Komatsu H, et al. Discovery of Chlorophyll *d* in *Acaryochloris marina* and Chlorophyll *f* in a Unicellular Cyanobacterium, Strain KC1, Isolated from Lake Biwa. J Phys Chem Biophys, 2014; 4:4.
6. Kobayashi M, van de Meent EJ, Amesz J, Ikegami I, Watanabe T. Bacteriochlorophyll *g* epimer as a possible reaction center component of heliobacteria. Biochim Biophys Acta, 1991; 1057: 89-96.
7. Watanabe T, Hongu A, Honda K, Nakazato M, Konno M, Saitoh S. Preparation of chlorophylls and pheophytins by isocratic liquid chromatography. Anal Chem, 1984; 56: 251-256.
8. French CS. The chlorophylls in vivo and in vitro. In: Springer V, ed. Encyclopedia of plant physiology, Berlin, 1960: Vol. 5, Part. 1, 252-280.
9. Akutsu S, Fujinuma D, Furukawa H, et al. Pigment analysis of a chlorophyll *f*-containing cyanobacterium strain KC1 isolated from Lake Biwa. Photomed Photobiol, 2011; 33: 35-40.
10. Kobayashi M, Watanabe T, Nakazato M, et al. Chlorophyll *a'*/P700 and pheophytin *a*/P680 stoichiometries in higher plants and cyanobacteria determined by HPLC analysis. Biochim Biophys Acta, 1988; 936: 81-89.
11. Nürnberg DJ, Morton J, Santabarbara S, et al. Photochemistry beyond the red limit in chlorophyll *f*–containing photosystems. Science, 2018; 360: 1210-1213.

Highly sensitive detection of the secondary electron acceptor, menaquinones-8 and 9, remaining in the purified reaction center core complex of *Heliobacterium modesticaldum*

Tomohito Mayumi[1], Tetsuko Nakaniwa[2], Kazuhito Inoue[3], Tomoya Katsuno[1], Zhengyang Tian[1], Hirozo Oh-oka[4], and Masami Kobayashi[1*]

[1] *Department of Materials Science, Faculty of Pure and Applied Sciences, University of Tsukuba, Ibaraki 350-8573, Japan*
[2] *Institute for Protein Research, Osaka University, Osaka 565-0871, Japan*
[3] *Department of Biological Sciences, Kanagawa University, 2946 Tsuchiya, Hiratsuka, Kanagawa 259-1293, Japan*
[4] *Department of Biological Sciences, Graduate School of Science, Osaka University, Osaka 560-0043, Japan*

***Corresponding author:**

Department of Materials Science, Faculty of Pure and Applied Sciences, University of Tsukuba, Ibaraki 350-8573, Japan
TEL: +81-298-53-6940
FAX: +81-298-53-4490
E-mail: masami@ims.tsukuba.ac.jp

ABSTRACT

Reversed-phase HPLC analyses showed that *Heliobacterium modesticaldum* had menaquinones-8 and 9; *Heliobacillus mobilis* contained MQs-7, 8 and 9; and *Heliobacterium fasciatum* possessed MQs-6 and 7, respectively. The MQ-pool size of (MQ-8 + MQ-9)/reaction center in *Hb. modesticaldum* was estimated to be ca. 20. It was shown that the RC of *Hb. modesticaldum* purified highly enough for crystallization had ca. 0.8 molecule of MQ in the ratio of MQ-9/8 ～ 4 still remaining in the HbRC core. Furthermore, the ratio found in the HbRC was almost the same as that observed in the cells, indicating MQs are loosely bound to the HbRC and are in thermal equilibrium between the HbRC and the MQ-pool in membranes. The result also suggests MQ to be an electron acceptor in the RC of *Hb. modesticaldum* and seems to support the idea that MQ also serves as a cyclic electron transfer component via the MQ-pool in membranes.

Keywords: bacteriochlorophyll *g*, chlorophyll *a*, heliobacteria, menaquinone, photosystem I

Abbreviations: BChl-bacteriochlorophyll; Chl-chlorophyll; HbRC-heliobacteria reaction center; HPLC-high performance liquid chromatography; MQ-menaquinone; P700-the primary electron donor of photosystem I; P798-the primary electron donor of heliobacteria; PhQ-phylloquinone; PS-photosystem; RC-reaction center

Introduction

Heliobacterium chlorum was first isolated serendipitously in 1981 from a soil sample collected in front of the Biology Department of Indiana University using an incorrectly prepared culture medium for other anoxygenic bacteria [1]. A new bacteriochlorophyll, BChl *g* esterified with farnesol, was discovered in this bacterium [2]. Bacteriochlorophyll *g* contains an 8-ethylidene group, and isomerization of the 8-ethylidene group of BChl *g* easily takes place to yield Chl *a* esterified with farnesol, Chl a_F [2-4], suggesting that BChl *g* is the most likely candidate for the ancestor of Chl *a* functioning in oxygenic photosynthesis [5].

The primary electron donor P798 (or P800) is a special pair of BChl *g*', a counterpart of P700, which is a pair of Chl *a* and Chl *a*', in PS I [5-10]. The primary electron acceptor A_0 is 8^1-hydroxy-Chl *a* (8^1-OH-Chl *a*), similar to A_0, Chl *a*, in PS I [5, 11]. The terminal electron acceptors F_X, F_A, and F_B are [4Fe-4S] type iron-sulfur clusters in PS I [12-15]. The identity of these components has been confirmed by the recent study on the 2.2-Å resolution crystal structure of the RC of *Heliobacterium modesticaldum* [16].

In contrast, the role of MQ in the HbRC has been controversial. Even from the crystal structure mentioned above, it has not been clear if quinones act in HbRC as an acceptor between A_0 and F_X, whereas A_1 in PS I has been identified as phylloquinone (PhQ) [9, 17-20]. In 1989, menaquinones (MQs)-7,8,9 and 10 were identified as the only quinones in *Heliobacterium chlorum* [21] and *Heliobacillus mobilis* [22]. Moreover, photoaccumulation of semiquinone was observed in the RCs of *Hb. chlorum*, *Hc. mobilis* and *Hb. Modesticaldum* [23-28], but no corresponding spectral change in the UV region was observed [29]. Furthermore, MQ can be extracted without effect of charge separation to FeS centers [30].

As mentioned above, no clear bindings of MQ

molecules were seen in the recently-revealed structure of the RC of *Hb. modesticaldum*, while the HbRC showed high similarity to PS I except for the absence of quinone [16]. However, there was an unassigned electron density to one side of A_0 that appeared to have an isoprenyl tail, suggesting the loss of intrinsic MQ during the preparation/ crystallization of the HbRC. Note that a weaker ESP signal was detected from the RC of *Hb. modesticaldum* purified high enough for crystallization, strongly suggesting that tiny amounts of MQ still remain in the purified HbRC. Therefore, it is interesting to clarify whether such traces of MQ still remain in the HbRC.

In this research, the HPLC system was modified to be capable of detecting trace amounts of MQ remaining in the purified RC core complexes of *Hb. Modesticaldum*.

Materials and Methods

Pigments extracted from cells and highly-purified RC core proteins by the procedure previously described [5, 31, 32] were injected onto a reversed-phase high-performance liquid chromatography (HPLC) column (Kaseisorb LC-ODS 2000-3, 250 × 4.6 mm) cooled to 277 K, and eluted isocratically with a degassed eluent of 86:13:1:0-3 ethanol/methanol/2-propanol/water, E*W(100/0-3), at a flow rate of 0.40 mL/min. Eluates were monitored in series with a JASCO UV-2070 detector (λ = 248 nm) and a Shimadzu multi-wavelength detector (SPD-M10A). The amount of pigments was determined by integrating the peak areas of the HPLC chromatograms, which were obtained using the molar extinction coefficients of individual compounds. Since BChl *g* and its 13^2-epimer, BChl *g'*, were easily converted to Chl *a*-like derivatives upon exposure to air, their values were summed up in the estimation of the total content of (B)Chl molecules. The detection system had been calibrated several times with known amounts of authentic BChl *g*, *g'*, Chl *a*, MQ-4 and MQ-7, where MQs-4 and 7 were purchased from Wako pure chemicals (Osaka, Japan). APCI-mass analyses of quinones were performed on a Shimadzu LCMS-2010EV spectrometer with an acceleration voltage of 4.5 kV. The highly-purified RC core protein was prepared after a gel filtration chromatography (Sephacryl S-200) of the RC core as described in [28].

Results and Discussion

Typical reversed-phase HPLC traces of acetone/ methanol extracts from cells of *Hb. modesticaldum*, *Heliobacillus mobilis* and *Heliobacterium fasciatum* are shown in Fig. 1, where MQs-6, 7, 8 and 9 were clearly separated with a simple isocratic eluent of E*W(100/3). The retention time for MQ-7 of *Hb. mobilis* and *Hb. fasciatum* was identical to that of authentic MQ-7

Four kinds of quinones found in three species of heliobacteria showed the same absorption spectra as that of authentic MQ-7, with all having absorption maxima at 248, 270 and 332 nm (Fig. 2), elucidating the presence of

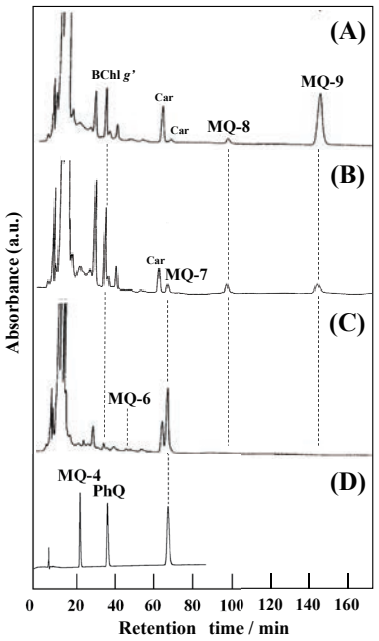

Fig. 1 Reversed-phase HPLC elution profiles of acetone/ methanol extracts of cells of (A) *Hb. modesticaldum*, (B) *Hc. Mobilis*, (C) *Hb. Fasciatum* and (D) a mixture of authentic MQ-4, PhQ and MQ-7. The pigments were eluted isocratically with a degassed solvent mixture of ethanol/methanol/2-propanol/ water (86/13/1/3), E*W(100/3), at a flow rate of 0.40 mL/min at 277 K and monitored with a photodiode array detector. Detection wavelength was 248 nm.

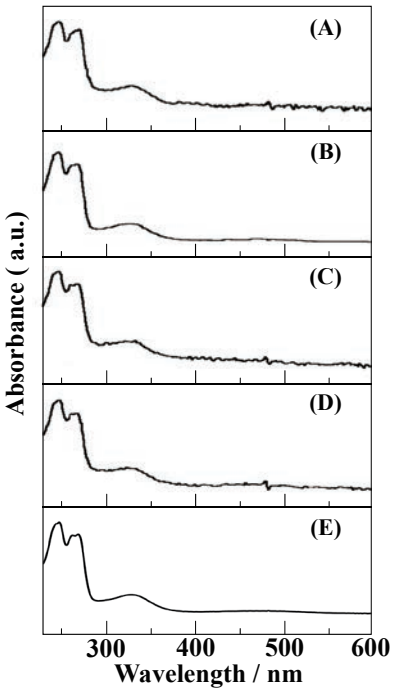

Fig. 2 Typical absorption spectra of (A) MQ-6 from *Hb. fasciatum*, (B) MQ-7 from *Hb. fasciatum* and *Hc. mobilis*, (C) MQ-8 from *Hc. Mobilis* and *Hb. Modesticaldum*, (D) MQ-9 from *Hc. mobilis* and *Hb. Modesticaldum* and (E) authentic MQ-7 in HPLC eluent measured by the photodiode array detector.

the same framework, naphthoquinone (see Fig. 6B).

APCI-mass spectra of MQs-6,7,8,9 of *Hb. Fasciatum*, *Hc. mobilis* and *Hb. Modesticaldum* are shown in Fig. 3. The positive ion APCI-mass spectrum of quinone of *Hb. fasciatum* showed a molecular ion peak $[M+H]^+$ at *m/z* 581.4 (Fig. 3A), which is identical to that of MQ-6 ($C_{41}H_{58}O_2$; mol wt = 580.4). The mass spectrum of quinone of *Hb. fasciatum* and *Hc. mobilis* showed a molecular ion peak $[M+H]^+$ at *m/z* 649.5 (Figs. 3A and B), which is in accord with that of MQ-7 ($C_{46}H_{64}O_2$; mol wt = 648.5). The mass spectrum of quinones of *Hc. mobilis* and *Hb. modesticaldum* showed a molecular ion peak $[M+H]^+$ at *m/z* 717.6 and 785.5 (Figs. 3B and C), coinciding with those of MQ-8 ($C_{51}H_{72}O_2$; mol wt = 716.6) and MQ-9 ($C_{56}H_{80}O_2$; mol wt = 784.6).

On the basis of (B)Chls/P798 = 60 [16], the molar ratios of MQ-8/P798 and MQ-9/P798 in the cells of *Hb. Modesticaldum* were calculated from the molar ratios of MQ-8/(B)Chls and MQ-9/(B)Chls to be 4.4 and 15.4, respectively, leading to the MQ-pool size = ca. 20 (Fig. 4A). If the HbRC contains two MQ molecules, the amount of MQ in the purified HbRC can be calculated to be one-tenth of 20 molecules of MQ found in MQ pool mentioned above. As seen in Fig. 4B, even such a small amount of MQ is a little difficult to be detected by our HPLC system with an isocratic eluent E*W(100/3) in Fig. 4B, but easily detected with E*W(100/1) in Fig. 4B', since by changing eluent from E*W(100/3) to E*W(100/1) the retention times of MQs get shorter, making the corresponding peaks sharper and higher.

Conversely, HbRC core proteins pure enough for crystallization showed terribly weak ESP signal, and hence the MQ/P798 ratio was assumed to be not 2 but below 0.5. While the system with eluent used in Fig. 4B' was not able to detect low levels of MQ quantitatively, if such trace amount of MQ must be detected quantitatively, a more sensitive system able to detect at least 0.2 level of MQ/P798, namely, one hundredth of the MQ pool size, is needed. Nevertheless, as presented in Fig. 4C, low level traces of MQ, MQ/P798 = 0.2, can be detected with a simple isocratic eluent of E*W(100/0) with a multi-wavelength detector. The inset chromatogram in the MQ-8 to 9 region in Fig. 4C was obtained with a monochromator, which is expected to allow more accurate detection of trace quantities of MQs remaining in the highly purified HbRC.

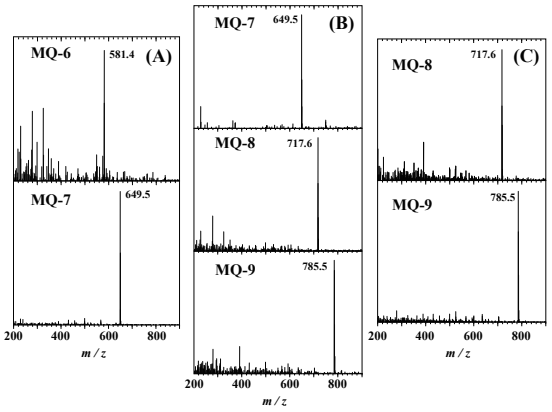

Fig. 3 A series of APCI-mass spectra of quinones of (A) *Hb. Fasciatum* , (B) *Hc. mobilis* and (C) *Hb. modesticaldum.*

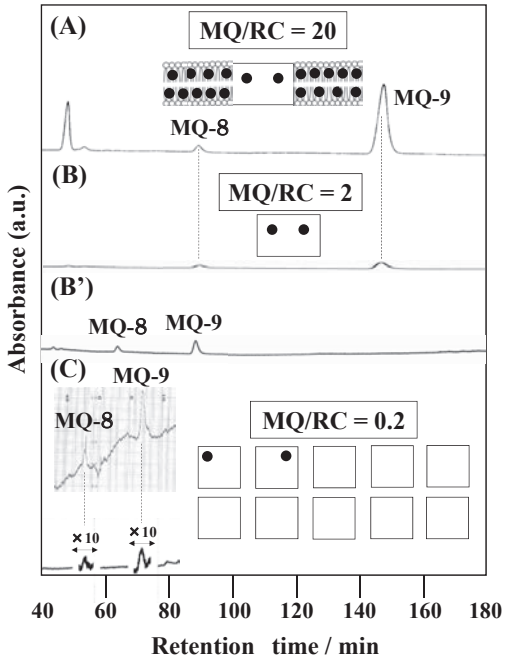

Fig. 4 Reversed-phase HPLC elution profiles of acetone/methanol extracts of *Hb. modesticaldum* cells. Cell suspension of (A) was diluted to 1/10 (B and B') and 1/100 (C). The degassed eluting solutions are (A and B) E*W(100/3), (B') E*W(100/1) and (C) E*W(100/0). Pigments are isocratically eluted and monitored with a photodiode array detector. The inset chromatogram in (C) in the region from MQ-8 to 9 was monitored with a monochromator. Detection wavelength was 248 nm.

On the other hand, a typical trace of acetone/methanol extract obtained by the modified HPLC system from the highly purified RC core complex of *Hb. modesticaldum* is illustrated in Fig. 5. Both MQs-8 and 9 were detected in the purified HbRC, and the corresponding two peaks showed the characteristic MQ absorption spectra with absorption maxima around 250, 270 and 330 nm (see inset in Fig. 5). On the basis of (B)Chls/P798 = 60 [16], the molar ratios of MQ-8/P798, MQ-9/P798 and (MQs-8 + 9)/P798 in the purified HbRC were calculated to be 0.14, 0.66 and 0.80, respectively (Table 1). The model for MQs/RC = 0.8 is schematically illustrated in the inset (Fig. 5), supposing there was no RC possessing two molecules of MQs. In this model, the 4/10 RC contains one MQ, the other 4/10 has one MQ in each opposing side, and the remaining 2/10 possesses no MQ. Unlike PS I, there was no tightly bound quinone in the recently published 2.2-Å resolution structure of the HbRC, but to one side of A_0 there was an unassigned electron density that appeared to have an isoprenyl tail [16]. A MQ molecule seems to fit into this density, visualizing where it might bind in the HbRC, hence the MQ binding site might be located in the

unassigned electron density [33].

It should be noted that some electron paramagnetic resonance experiments have been interpreted as evidence for the involvement of a semiquinone species during forward ET within the HbRC [25-28]. Additionally, a new type of ESP signal in the RC core complex of *Hb. modesticaldum* has been recently reported and ascribed to the $P798^{+}A_1^{-}$ state, whereas MQ in the HbRC is somewhat different from PhQ functioning as A_1 in the PS I RC, in terms of the molecular orientation and/or distance [26-28].

What is more, the molar ratio of MQ-9/8 = 3.8 found in the purified HbRC is almost the same as that found in the cells, namely, 3.6 (Table 1), strongly indicating that MQs are loosely bound to and dissociate from HbRC rather easily [22, 34, 35], which most probably brings MQ to the thermal equilibrium between the HbRC and the MQ-pool in membranes (Fig. 6A). This hypothesis strongly supports the idea that MQ also serves as an alternate cyclic electron transfer component via MQ-pool in membranes [33], similar to the mobile quinones for the type-II RCs. It is worth mentioning that the HbRC preferentially reduce soluble electron acceptors (e.g. ferredoxins, Fd) in low light, but switches to reducing lipophilic quinones in high light, when the soluble acceptor pool becomes full [33, 36]. As a result, the HbRC may represent a functional evolutionary intermediate between the type I and II RC [33].

Similarly, the electron acceptor A_1 in PS I has been

Table. 1 Stoichiometries of MQs/RC and MQ-9/MQ-8 in the cells and the RC of *Hb. modesticaldum*

	MQ-8/RC	MQ-9/RC	MQ/RC	MQ-9/MQ-8
cells	**4.4 ± 1.1 (*n* = 8)**	**15.4 ± 1.1 (*n* = 8)**	**19.9 ± 3.2 (*n* = 8)**	**3.6 ± 0.5 (*n* = 8)**
RC	**0.14 ± 0.02 (*n* = 5)**	**0.66 ± 0.05 (*n* = 6)**	**0.80 ± 0.06 (*n* = 5)**	**3.8 ± 0.6 (*n* = 5)**

MQ-8/RC and MQ-9/RC: calculated from MQ-8/(B)Chls and MQ-9/(B)Chls on the basis of (B)Chls/RC = 60 [16].
n: numbers of analyses.

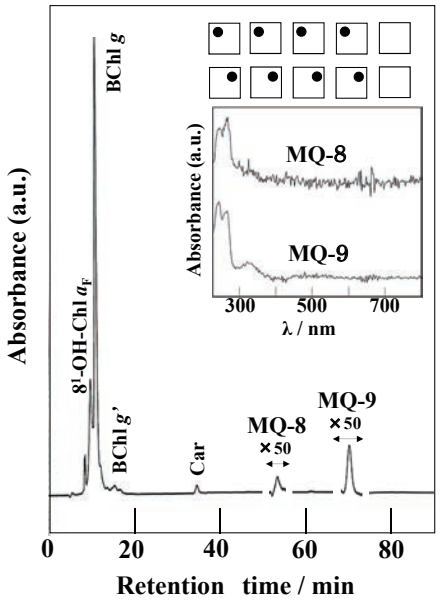

Fig. 5 Typical HPLC elution profile of acetone/methanol extract of the purified RC core complexes of *Hb. modesticaldum*. The extracted pigments were eluted isocratically with a degassed solvent mixture of E*W(100/0) at a flow rate of 0.40 mL min^{-1} cooled to 277 K and monitored with a photodiode array detector. Detection wavelength was 248 nm. Absorption spectra of MQs-8 and 9 in an HPLC eluent measured by the photodiode array detector are inset into the chromatogram. Schematic model for the purified RC showing the ratio of MQ/RC = 0.8 is also inset into the chromatogram.

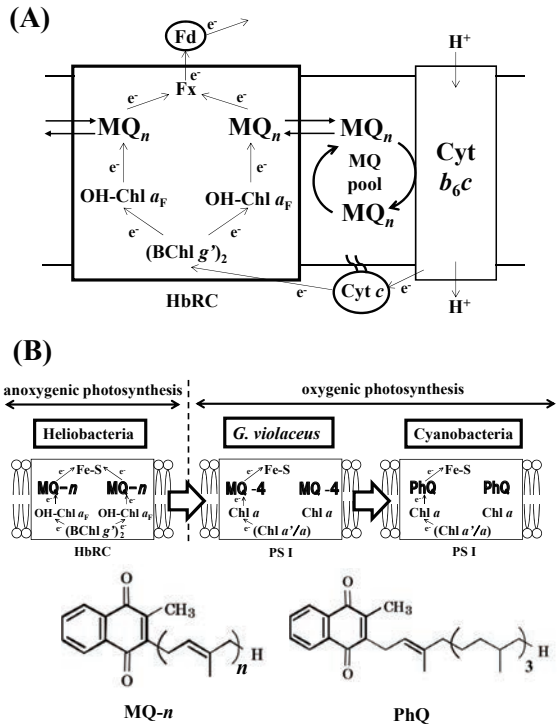

Fig. 6 (A) Proposed model for electron transfer scheme via two pathways in heliobacteria (adapted from Kashey et al. 2018). One is from F_X to cellular ferredoxin (Fd), and the other is from HbRC to Cyt*b*6 via internal MQ and MQ-pool. (B) Schematic illustration of succession of cofactors in the PS I-type RCs based on the molecular structures of key chlorophylls (BChl *g*, *g*'→Chl *a*, *a*') and quinones (MQ→PhQ) (adapted from Ohashi et al.2010).

identified as PhQ (Fig. 6B) in the mid-1980s [17, 18], and its function between A_0 and F_X has been extensively documented [19, 20]. The HbRC has been assumed to be one of the oldest type-I RC remaining the feature of the ancestral RC [37-39]. Consequently, the study on MQs in the HbRC will supply a clue to understand the evolution of the type-I RCs, since quinone functions differ significantly between the type-I and II RCs [5, 20, 40, 41].

In 1972, *Gloeobacter violaceus* was first isolated from the surface of a limestone rock collected in the Kernwald in Switzerland [42], *Gloeobacter violaceus* is a unicellular cyanobacterium of unusual structure: it lacks thylakoid membranes in the cytoplasm and the photosystems are located on the cytoplasmic membrane. *Gloeobacter violaceus* is assigned to an early-branched species in the phylogenetic tree of cyanobacteria based on the 16S rRNA sequence [43] and thus to a connecting site between the anoxygenic photosynthesis and oxygenic photosynthesis (Fig. 6B).

A heterodimer of Chl *a* and *a'* functions as P700 in the heterodimeric PS I RC of *G. violaceus* and typical cyanobacteria (Fig. 6B), and Phe *a* functions as the primary electron acceptor in the PS II RC [5, 32, 44], so no chemical evolution of chlorophylls occurred during the biological evolution from *G. violaceus* to typical cyanobacteria.

Notwithstanding, when the attention is turned to quinones, A_1 of PS I in *G. violaceus* is not PhQ but MQ-4 (Fig. 6B) [32], indicating that the molecular evolution of A_1 quinones in the type-I RCs did not happen during the evolution from anoxygenic heliobacteria into an early-diverging oxygenic cyanobacterium, e.g. *G. violaceus*, and that the molecular evolution of quinone (reduction of long chain of MQ-4 to yield PhQ) most likely took place after the birth of typical cyanobacteria (Fig. 6B). To the authors' knowledge, at least three species, a primitive cyanobacterium *G. violaceus*, a primitive unicellular red alga *Cyanidium caldarium* [45] and a marine centric diatom *Chaetoceros gracilis* [46] utilize MQ instead of PhQ as A_1, strongly indicating that the biological evolution of oxygenic photosynthesis from primitive cyanobacteria, e.g. *G. violaceus*, to typical cyanobacteria followed by algae is complex with regards to A_1. As the second electron acceptor, A_1, *G. Violaceus* and typical cyanobacteria utilize singular quinone, MQ-4 and PhQ, respectively (Fig. 6B), while heliobacteria use plural MQs, MQs-6, 7, 8 and 9 (Fig. 1). We cannot explain why several MQs are used in heliobacteria, and the studies of biosynthesis of MQs in heliobacteria are awaited.

As illustrated in Fig. 6B, Chl *a*-derivatives function as A_0 in the HbRC, in the PS I RC of *G. Violaceus* and typical cyanobacteria. When the cofactors in the RCs of heliobacteria and PS I RC of the primitive cyanobacterium *G. violaceus* are compared, a significant difference is seen in the primary electron donors: (BChl *g'*)$_2$ in heliobacteria and Chl *a/a'* in PS I. The conversion of BChl *g'* to Chl *a'* can be done by the isomerization of BChl *g'* under weak acidic conditions [4]. Subsequent conversion of (Chl *a'*)$_2$ → Chl *a/a'*, a homodimeric special pair to a heterodimeric special pair, can be simply made by epimerization of one molecule of Chl *a'* yielding Chl *a*, which is plausibly concurrent with the evolution from the homodimeric RC to the heterodimeric RC. Accordingly, heliobacteria are the most likely candidate for the ancestor of the type-I RCs (Fig. 6B).

It may be of interest to mention the striking structural similarity among the cores of the type-I and II RCs, leading to the idea that both types of RCs share a common evolutionary origin [33, 47, 48], and the original RC was almost surely homodimeric like HbRC [33]. As suggested above, there might be two possible cyclic electron transport pathways in heliobacteria (Fig. 6A), where a larger cycle using Fd resembles the cycle in PS I and a smaller cycle bears a striking resemblance to the cycle in purple bacteria. The smaller cycle may be the ancestral one and the larger cycle would represent a new pathway allowed by the ability of the type-I RCs to reduce Fd via FeX in the HbRC, which has opened up a new cycle involving NADH dehydrogenase and additional proton pumping with a concomitant increase in ATP production [33].

To clarify whether MQs are present and function as A_1 in the HbRC, further crystal structure studies of HbRC are eagerly awaited.

References

1. Gest H. Discovery of the heliobacteria. Photosynth Res 1994;41:17-21.
2. Brockmann H Jr, Lipinski A. Bacteriochlorophyll *g*. A new bacterio-chlorophyll from *Heliobacterium chlorum*. Arch Microbiol 1983;136:17-19.
3. Michalski TJ, Hunt JE, Bowman MK, et al. Bacteriopheophytin *g*: properties and some speculations on a possible primary role for bacteriochlorophylls *b* and *g* in the biosynthesis of chlorophylls. Proc Natl Acad Sci USA 1987;84:2570-2574.
4. Kobayashi M, Hamano T, Akiyama M, et al. Light-independent isomerization of bacterio-chlorophyll *g* to chlorophyll *a* catalyzed by weak acid *in vitro*. Anal Chim Acta 1998;365:199-203.
5. Ohashi S, Iemura T, Okada N, et al. An overview on chlorophylls and quinones in the photosystem I-type reaction centers. Photosynth Res 2010;104:305−319.
6. Kobayashi M, Watanabe T, Nakazato M, et al. Chlorophyll *a'*/P-700 and pheophytin *a*/P-680 stoichiometries in higher plants and cyanobacteria determined by HPLC analysis. Biochim Biophys Acta 1988;936:81-89.
7. Kobayashi M, Van de Meent EJ, Amesz J, Ikegami I, Watanabe T. Bacteriochlorophyll *g* epimer as a possible reaction center component of heliobacteria. Biochim Biophys Acta 1991;1057:89-96.
8. Kobayashi M, Watanabe T, Ikegami I, Van de Meent

EJ, Amesz J. Enrichment of bacteriochlorophyll *g'* in membranes of *Heliobacterium chlorum* by ether extraction - Unequivocal evidence for its existence *in vivo*. FEBS Lett 1991;284:129-131.
9. Jordan P, Fromme P, Witt HT, Klukas O, Saenger W, Krauβ N. Three-dimensional structure of cyanobacterial photosystem I at 2.5 Å resolution. Nature 2001;411:909-917.
10. Rigby SEJ, Evans MCW, Heathcote P. Electron nuclear double resonance (ENDOR) spectroscopy of radicals in photosystem I and related Type 1 photosynthetic reaction centres. Biochim Biophys Acta 2001;1507:247-259.
11. Van de Meent EJ, Kobayashi M, Erkelens C, Van Veelen PA, Amesz J, Watanabe T. Identification of 8^1-hydroxychlorophyll *a* as a functional reaction center pigment in heliobacteria. Biochim Biophys Acta 1991;1058:356-362.
12. Nitschke W, Setif P, Liebl U, Feiler U, Rutherford AW. Reaction center photochemistry of *Heliobacterium chlorum*. Biochemistry 1990;29:11079−11088
13. Heinnickel M, Agalarov R, Svensen N, Krebs C, Golbeck JH. Identification of F_X in the heliobacterial reaction center as a [4Fe-4S] cluster with an $S = 3/2$ ground spin state. Biochemistry 2006;45:6756−6764.
14. Heinnickel M, Shen GZ, Golbeck JH. Identification and characterization of PshB, the dicluster ferredoxin that harbors the terminal electron acceptors F_A and F_B in *Heliobacterium modesticaldum*. Biochemistry 2007;46:2530−2536.
15. Kondo T, Matsuoka M, Azai C, Itoh S, Oh-Oka H. Orientations of iron-sulfur clusters F_A and F_B in the homodimeric type-I photosynthetic reaction center of *Heliobacterium modesticaldum*. J Phys Chem B 2016;120:4204−4212.
16. Gisriel C, Sarrou I, Ferlez B, Golbeck JH, Redding KE, Fromme R. Structure of a symmetric photosynthetic reaction centerphotosystem. Science 2017;357:1021−1025.
17. Takahashi Y, Hirata K, Katoh S. Multiple forms of P700-chlorophyll *a*-protein complexes from *Synechococcus* sp.: the iron, quinone and carotenoid contents. Photosynth Res 1985;6:183-192.
18. Schoeder H-U, Lockau W. Phylloquinone copurifies with the large subunit of photosystem I. FEBS Lett 1986;199:23-27.
19. Brettel K. Electron transfer and arrangement of the redox cofactors in photosystem I. Biochim Biohys Acta 1997;1318:322-373.
20. Itoh S, Iwaki M, Ikegami I. Modification of photosystem I reaction center by the extraction and exchange of chlorophylls and quinones. Biochim Biophys Acta 2001;1507:115-138.
21. Hiraishi A. Occurrence of menaquinone as the sole isoprenoid quinone in the photosynthetic bacterium *Heliobacterium chlorum*. Arch Microbiol 1989;151:378-379.
22. Trost JT, Blankenship RE. Isolation of a photoactive photosynthetic reaction center-core antenna complex from *Heliobacillus mobilis*. Biochemistry 1989;28:9898-9904.
23. Brok M, Vasmel H, Horikx JTG, Hoff AJ. Electron transport components of *Heliobacterium chlorum* investigated by EPR spectroscopy at 9 and 35 GHz. FEBS Lett 1986;194:322-326.
24. Trost JT, Brune DC, Blankenship RE. Protein sequences and redox titrations indicate that the electron acceptors in reaction centers from heliobacteria are similar to Photosystem I. Photosynth Res 1992;32:11-22.
25. Muhiuddin IP, Rigby SEJ, Evans MCW, Amesz J, Heathcote P. ENDOR and special TRIPLE resonance spectroscopy of photoaccumulated semiquinone electron acceptors in the reaction centers of green sulfur bacteria and heliobacteria. Biochemistry 1999;38:7159-7167.
26. Miyamoto R, Mino H, Kondo T, Itoh S, Oh-oka H. An electron spin-polarized signal of the $P800^+A_1(Q)^-$ state in the homodimeric reaction center core complex of *Heliobacterium modesticaldum*. Biochemistry 2008;47:4386-4393.
27. Kondo T, Itoh S, Matsuoka M, Azai C, Oh-oka H. Menaquinone as the secondary electron acceptor in the type I homodimeric photosynthetic reaction center of *Heliobacterium modesticaldum*. J Phys Chem B 2015;119:8480−8489.
28. Kondo T, Matsuoka M, Azai C, Kobayashi M, Itoh S, Oh-oka H. Light-induced electron spin-polarized (ESP) EPR signal of the $P800^+$ menaquinone$^-$ radical pair state in oriented membranes of *Heliobacterium modesticaldum*: role/location of menaquinone in the homodimeric type I reaction center. J Phys Chem B 2018;122:2536-2543.
29. Brettel K, Leibl W, Liebl U. Electron transfer in the heliobacterial reaction center: evidence against a quinone-type electron acceptor functioning analogous to A_1 in photosystem I. Biochim Biophys Acta 1998;1363:175-181.
30. Kleinherenbrink FAM, Ikegami I, Haraishi A, Otte SCM, Amesz J. Electron transfer in menaquinone-depleted membranes of *Heliobacterium chlorum*. Biochim Biophys Acta 1993;1142:69-73.
31. Akiyama M, Miyashita H, Watanabe T, Kise H, Miyachi S, Kobayashi M. Detection of chlorophyll *d'* and pheophytin a in a chlorophyll *d*-dominating oxygenic photosynthetic prokaryote *Acaryochloris marina*. Anal Sci 2001;17:205-208.
32. Mimuro M, Tsuchiya T, Inoue H, et al. The secondary electron acceptor of photosystem I in *Gloeobacter violaceus* PCC7421 is menaquinone-4 that is synthesized by a unique but unknown pathway. FEBS Lett 2005;579:3493-3496.
33. Kashey TS, Luu DD, Cowgill JC, Baker PL, Redding KE. Light-driven quinone reduction in heliobacterial

membranes. Photosynth Res 2018;138:1-9.
34. Sarrou I, Khan Z, Cowgill J, et al. Purification of the photosynthetic reaction center from *Heliobacterium modesticaldum*. Photosynth Res 2012;111:291−302.
35. Chauvet A, Sarrou J, Lin S, et al. Temporal and spectral characterization of the photosynthetic reaction center from *Heliobacterium modesticaldum*. Photosynth Res 2013;116:1-9.
36. Redding KE, Sarrou I, Rappaport F, Santabarbara S, Lin S, Reifschneider KT. Modulation of the fluorescence yield in heliobacterial cells by induction of charge recombination in the photosynthetic reaction center. Photosynth Res 2014;120:221–235.
37. Vermaas WFJ. Evolution of heliobacteria - Implications for photosynthetic reaction center complexes. Photosynth Res 1994;41:285−294.
38. Olson JM, Blankenship RE. Thinking about the evolution of photosynthesis. Photosynth Res 2004;80:373−386.
39. Sadekar S, Raymond J, Blankenship RE. Conservation of distantly related membrane proteins: Photosynthetic reaction centers share a common structural core. Mol Biol Evol 2006;23:2001−2007.
40. Srinivasan N, Golbeck JH. Protein−cofactor interactions in bioenergetic complexes: The role of the A_{1A} and A_{1B} phylloquinones in Photosystem I. Biochim Biophys Acta 2009; 1787;1057− 1088.
41. Müh F, Glöckner C, Hellmich J, Zouni A. Light-induced quinone reduction in photosystem II. Biochim Biophys Acta 2012;1817;44−65.
42. Rippka R, Waterbury J, Cohen-Bazire G. A cyanobacterium which lacks thylakoids. Arch Microbiol 1974;100:419-436.
43. Nakamura Y, Kaneko T, Sato S, et al. Complete genome structure of *Gloeobacter violaceus* PCC 7421, a cyanobacterium that lacks thylakoids. DNA Res 2003;10(4):137-145.
44. Ohashi S, Tsuchiya T, Iwamoto K, et al. Succession of co-factors in photosystem I. In: Allen JF, Gantt E, Golbeck JH, Osmond B, eds. Photosynthesis: Energy from the Sun. Dordrecht: Springer, 2008;1177-1180.
45. Yoshida E, Nakamura A, Watanabe T. Reversed-phase HPLC determination of chlorophyll *a′* and naphthoquinones in photosystem I of red algae: Existence of two menaquinone-4 molecules in photosystem I of *Cyanidium caldarium*. Anal Sci 2003;19:1001-1005.
46. Ikeda Y, Komura M, Watanabe M, et al. Photosystem I complexes associated with fucoxanthin-chlorophyll-binding proteins from a marine centric diatom, *Chaetoceros gracilis.* Biochim Biophys Acta 2008;1777:351-361.
47. Rutherford AW, Nitschke W. Photosystem II and the quinone-iron-containing reaction centers: comparisons and evolutionary perspectives. In: Baltscheffsky H, ed. Origin and evolution of biological energy conversion. New York: VCH Publishers, 1996;143–175.
48. Schubert WD, Klukas O, Saenger W, Witt HT, Fromme P, Krauss N. A common ancestor for oxygenic and anoxygenic photosynthetic systems: a comparison based on the structural model of photosystem I. J Mol Biol 1998;280:297–314.

Cellular uptake of aggregates consisting of oligodeoxynucleotides bearing alkyl chain at strand end

Akihiro Kitao, Ryohsuke Kurihara, and Kazuhito Tanabe*

Department of Chemistry and Biological Science, College of Science and Engineering, Aoyama Gakuin University, 5-10-1 Fuchinobe, Chuo-ku, Sagamihara, Kanagawa 252-5258, Japan

Abstract

Aggregate consisted of amphiphilic DNA strand showed favorable properties as biofunctional molecule in living cells. We prepared oligodeoxynucleotides (ODNs) bearing alkyl chain at strand end, and characterized their chemical and biological properties. The ODNs formed aggregate and smoothly penetrated the cell membrane. In addition, introducing methyl group at phosphate unit resulted in an acceleration of cellular uptake.

INTRODUCTION

Functional oligonucleotides show several functions in living cells.[1-4] For example, nucleic acids medicine binds with the target mRNA in the cells to suppress gene expression. DNA or RNA aptamers bind with small molecules or proteins to regulate their functions. However, these oligonucleotides have several drawbacks. First, their anionic properties inhibit the penetration of cell membrane, although they have to function inside the cells. Second, they are easily degraded by nuclease in the cells, and therefore, they are unstable in the living systems. To solve these problems, several transfection reagents such as cationic lipid and functional polymers have been developed to protect and deliver them into the target cells.

We have developed amphiphilic oligonucleotides and characterized their chemical and biological properties.[5-7] We revealed that the amphiphilic oligonucleotides bearing hydrophobic fluorescent molecules formed aggregate in aqueous solution and the aggregate smoothly penetrated the cell membrane and accumulated in the cells. Furthermore, the aggregate consisting of double-stranded RNA effectively regulated gene expression. Thus, aggregate consisting of amphiphilic oligonucleotides showed favorable properties as biofunctional molecules with high biological stability and cell permeability. These research contexts prompted us to evaluate the relationships between structures of modified oligonucleotides and their cellular uptake. Herein, we prepared other oligonucleotides that had hydrophobic alkyl chain at strand end and evaluated their cellular uptake.

MATERIALS AND METHODS

Synthesis of ODN 1 (General procedure for the synthesis of oligonucleotides). *N*,*N*-diisopropylethylamine (0.129 g, 1.00 mmol) and 2-cyanoethyldiisopropyl-chlorophosphoramidite (94.6 mg, 0.400 mmol) were added to 1-eicosanol (59.7 mg, 0.200 mmol) in CH_2Cl_2 (2 mL) and stirred for 2 h at room temperature. After the reaction, the reaction mixture was filtered and placed on DNA synthesizer. After automated DNA synthesis, crude ODN 1 was purified by reversed phase HPLC. The purity and concentration of the oligomers were determined by complete digestion with AP, P1 and phosphodiesteraseI at 37 ℃ for 16 h. Identities of synthesized oligomers were confirmed by MALDI-TOF mass spectrometry (**ODN 1**: $[M\text{-}H]^-$ calcd 1818.52, found 1819.02.

Measurement of fluorescence spectra. To form the aggregate, indicated concentrations of oligonucleotides in phosphate sodium buffer (5 mM, pH 7.0) were added to nile red (5 μM) in acetonitrile. After the removal of solvent in vacuo, the resulting mixture was dissolved in water to form the aggregate and measure the fluorescence spectra. We measured the spectra by means of excitation wavelength at 552 nm for nile red.

Cellular imaging by confocal laser scanning microscopy. For confocal laser scanning microscopy, 1×10^4 A549 cells were seeded in 96 well plates, then incubated at 37 ℃ for 24 h. The medium from each well was then removed, and cells were fed with medium (100 μL) containing oligonucleotides. After 24h of incubation, the cells were washed three times with phosphate-buffered saline (PBS), and then imaged using excitation at 488 nm. Confocal fluorescence microscopy was performed on a Nikon C2 laser scanning confocal system.

RESULTS AND DISCUSSION

Initially, to verify the aggregate formation of amphiphilic ODNs, we prepared two ODNs (ODN 1 and 2 in Figure 1A) bearing alkyl chain at the strand end by automated DNA synthesis and characterized their aggregation in aqueous solution. We identified aggregate formation by measuring the fluorescence of nile red dye. Nile red showed negligible emission in aqueous suspension, while encapsulation of nile red into aggregates consisting of amphiphilic molecules resulted in a robust fluorescence, even in aqueous solution. Thus, we evaluated the aggregate formation of ODNs by monitoring fluorescence of nile red. As shown in Figure 1B, negligible emission of nile red was observed around 640 nm in the

absence of ODN 1, while the addition of ODN 1 led to a significant enhancement of the emission, indicating that ODN 1 formed aggregates that encapsulated nile red in their hydrophobic core. The CAC value, which indicates the concentration of amphiphilies above which aggregate formation occurred, was determined to be 89 μM for ODN 1. We also observed similar aggregate formation of ODN 2, the CAC value of which was estimated as 45 μM.

We then performed cellular experiments of ODN 1 and ODN 2 using a human cell line of lung adenocarcinoma, A549, to evaluate their cellular uptake without transfection reagents. We employed fluorophore (FAM)-labeled ODNs (ODN 1F and ODN 2F) and blended it with normal ODNs for tracking their behavior in cells. A549 cells were incubated with mixture of ODN 1 and ODN 1F at the concentration that was sufficient to form aggregates (200 μM ODN 1 + 5 μM ODN 1F) and the fluorescence emission of FAM from the cells was imaged using confocal microscopy. As shown in Figure 1C, high emission levels were observed from the cells, indicating that ODN 1 aggregates penetrated cell membranes smoothly at this concentration. On the other hand, the cells incubated in the presence of ODN 2 showed weak emission. Thus, the aggregate penetrated cell membrane and accumulated in the cells, but strand length seemed to affect the cellular uptake, importantly.

In order to improve the cellular uptake of ODN 2, we next changed the chemical structure of ODN 2. Because we speculated that the high hydrophilicity of ODN 2 due to the long strand length prevented the internalization of ODN 2, we next replaced a phosphate group by a methyl phosphate to increase the hydrophobicity of the strand. We prepared ODN 3 with a methyl phosphate unit and alkyl chain at strand end and characterized its behavior. Fluorescence measurement experiments using nile red molecules in the presence of ODN 3 revealed that they formed aggregates in aqueous solution with a CAC value of 10 μM. The observation of the cellular uptake of ODN 3 aggregate by confocal microscopy showed that its aggregates smoothly penetrated the cell membrane and showed bright emission in A549 cells. These results strongly indicate that the balance of hydrophobic unit and hydrophilic unit was responsible for the cellular uptake of the aggregate.

CONCLUSION

In conclusion, we designed amphiphilic ODNs and characterized their behaviors in living cells. We prepared ODNs bearing alkyl chain at strand end, which formed aggregate in aqueous solution. The aggregate of ODNs penetrated cell membrane without any additives. In particular, modified ODNs with methyl phosphate group showed efficient cellular uptake. Thus, the aggregate formation of ODNs are promising candidate to deliver ODNs into living cells.

REFERENCES

(1) Seeman, N. C. DNA in a material world. *Nature*, 2003; 421: 427-431.

(2) Jiang, Q., Zhao, S., Liu, J., Song, L., Wang, Z.-G., Ding, B. Rationally designed DNA-based nanocarriers. *Adv. Drug. Deliv. Rev. in press*.

(3) Tang, Y., Ge, B., Sen, D., Yu, H. -Z. Functional DNA switches: rational design and electrochemical signaling. *Chem. Soc. Rev.*, 2014; 43: 518-529.

(4) Li, H., Lee, T., Dziubla, T., Pi, F., Guo, S., Xu, J., Li, C., Haque, F., Liang, X.-J., Guo, P. RNA as a Stable Polymer to Build Controllable and Defined Nanostructures for Material and Biomedical Applications. *Nano Today*, 2015; 10: 631-655.

(5) Asahi, W., Kurihara, R., Takeyama, K., Umehara, Y., Kimura, Y., Kondo, T., Tanabe, K. Aggregate formation of BODIPY-tethered oligonucleotides that led to efficient intracellular penetration and gene regulation. *ACS Applied Bio Materials*, 2019; 2: 4456-4463.

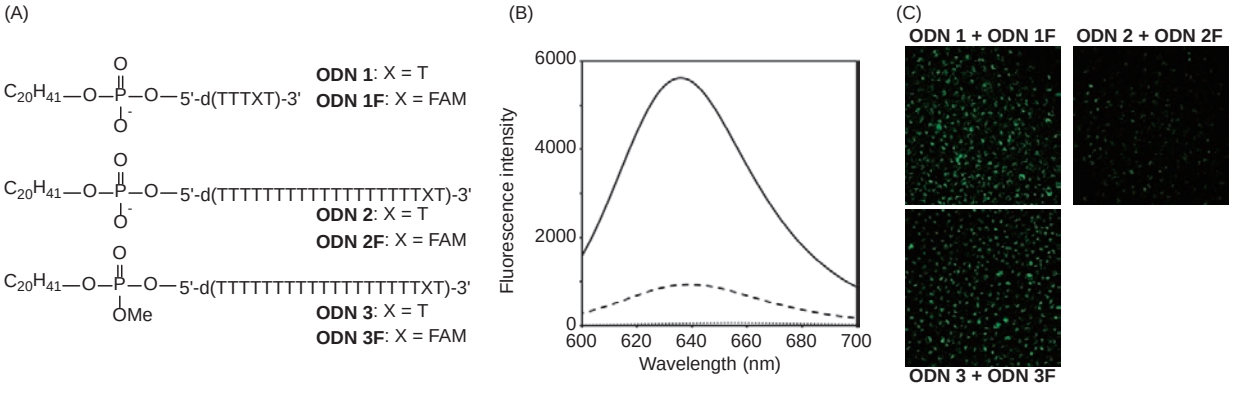

Figure 1. (A) Chemical structures of oligodeoxynucleotides used in this study. (B) Formation of aggregates from ODN 1 and encapsulation of nile red. Fluorescence spectra of nile red (5 μM) in the presence of ODN 1 (0 μM: dotted line, 100 μM: dashed line, 200 μM: solid line). The fluorescence spectra were measured at 552 nm excitation. (C) Cellular uptake of modified ODNs in A549 cells. After administration of the ODNs (200 μM ODN 1, 2 or 3 + 5 μM ODN 1F, 2F or 3F) for 24 h, the cells were washed and immediately subjected to confocal microscopy (excitation at 488 nm and emission at 500-550 nm).

(6) Misu, S., Kurihara, R., Kaimuma, R., Sato, R., Nishihara, T., Tanabe, K. Hybridization of Oligonucleotides with Hydrophobic Peptide Nucleic Acids Assists Their Cellular Uptake via Aggregate Formation. *ChemBioChem in press*.
(7) Yoshihara, K., Takagi, K., Son, A., Kurihara, R., Tanabe, K. Aggregate formation of oligonucleotides that assisted molecular imaging for tracking of oxygen status in tumor tissue. *ChemBioChem* 2017; *18*: 1650-1658.

Electrostatic Interaction with Anionic Polymer Activates Berberine Photosensitizer

Kazutaka Hirakawa[1,2,*], Mariko Yamada[1], Shigetoshi Okazaki[3], Morihiko Hamada[4], and Yasuhiro Kobori[4,5]

[1] *Applied Chemistry and Biochemical Engineering Course, Department of Engineering, Graduate School of Integrated Science and Technology, Shizuoka University, Johoku 3-5-1, Naka-ku, Hamamatsu, Shizuoka 432-8561, Japan*
[2] *Department of Optoelectronics and Nanostructure Science, Graduate School of Science and Technology, Shizuoka University, Johoku 3-5-1, Naka-ku, Hamamatsu, Shizuoka 432-8561, Japan*
[3] *Preeminent Medical Photonics Education & Research Center, Hamamatsu University School of Medicine, Handayama 1-20-1, Higashi-ku, Hamamatsu, Shizuoka 431-3192, Japan*
[4] *Laser Molecular Photoscience Laboratory, Molecular Photoscience Research Center, Kobe University, 1-1 Rokkodai, Nada-ku, Kobe 657-8501, Japan*
[5] *Department of Chemistry, Graduate School of Science, Kobe University, 1-1 Rokkodai, Nada-ku, Kobe 657-8501, Japan*

***Corresponding author:** Kazutaka Hirakawa
Applied Chemistry and Biochemical Engineering Course, Department of Engineering, Graduate School of Integrated Science and Technology, Shizuoka University, Johoku 3-5-1, Naka-ku, Hamamatsu, Shizuoka 432-8561, Japan
Tel/Fax: +81-53-478-1287, E-mail: hirakawa.kazutaka@shizuoka.ac.jp

Abstract: Electrostatic interaction with polystyrene sulfonate, a water-soluble anionic polymer, suppressed the self-quenching of photoexcited berberine, an alkaloid. Neutral water-soluble polymers and alginate, a naturally occurring anionic polymer, showed no or little effect on the photochemical property of berberine. Polystyrene sulfonate significantly increased the lifetime of photoexcited berberine, leading to the improved quantum yield of singlet oxygen generation. Polystyrene sulfonate's activity control of berberine photosensitizer may have application for photomedicine.

Keywords: Berberine, Photosensitizer, Polystyrene sulfonate, Electrostatic interaction, Singlet oxygen

INTRODUCTION

Various natural compounds, such as plant extracts, demonstrate photosensitizing activity [1]. Control of the phototoxic activity of naturally occurring compounds through interaction with biomolecules [2] or safety substances [3] may be applied for photomedicine. Photodynamic therapy (PDT), a less-invasive cancer therapy [4,5] and photo-sterilization [6] using a non-thermal visible light, is one of the most important examples of photomedicine. Berberine (5,6-dihydro-9,10-dimethoxybenzo[g]-1,3-benzodioxolo[5,6-a] quinolizinium, Fig. 1), an alkaloid isolated from Goldenseal (*Hydrastis canadensis* L.), is itself a safety compound in dark condition [7]. Antibacterial, anti-inflammatory, and antidiarrheal effects are important characteristics of berberine [8,9]. The photoexcited state (singlet excited (S_1) state) of berberine is effectively quenched through intramolecular electron transfer [10]. This quenching effect suppresses the phototoxic activity of berberine in aqueous media [11]. However, an electrostatic interaction with DNA [2,10] or inclusion complexation with cyclodextrin [3,12,13] enhances the fluorescence quantum yield [2,3,10,12,13] and singlet oxygen ($^1O_2$)-generating [2,3,10] activity of berberine. The improved photosensitization of berberine with safety materials may have application for photomedicine. This study examines the activity control of berberine photosensitizer through an interaction with water-soluble polymers (Fig. 1).

EXPERIMENTAL

Agarose XP, berberine chloride, and sodium alginate were purchased from FUJIFILM Wako Pure Chemical Co., Ltd. (Tokyo Japan). Polyvinylpyrrolidone K 30 (PVP) was from Tokyo Chemical Industry Co., Ltd. (Tokyo Japan). Sodium polystyrene sulfonate (PSS) was from Sigma-Aldrich Co. LLC. (St. Louis, MO, U.S.A.). These chemical agents were used as received. Berberine was mixed with a polymer in a 10 mM sodium phosphate buffer (pH 7.6) to measure absorption and fluorescence spectra. Fluorescence lifetime (τ_f) was measured with a Fluorescence Lifetime System TemPro (HORIBA, Kyoto, Japan) and the fluorescence quantum yield (Φ_f) was measured with an absolute photoluminescence quantum yield measurement system (C9920-02, Hamamatsu Photonics K.K., Hamamatsu, Japan). The excitation wavelength for the fluorescence measurements was 394

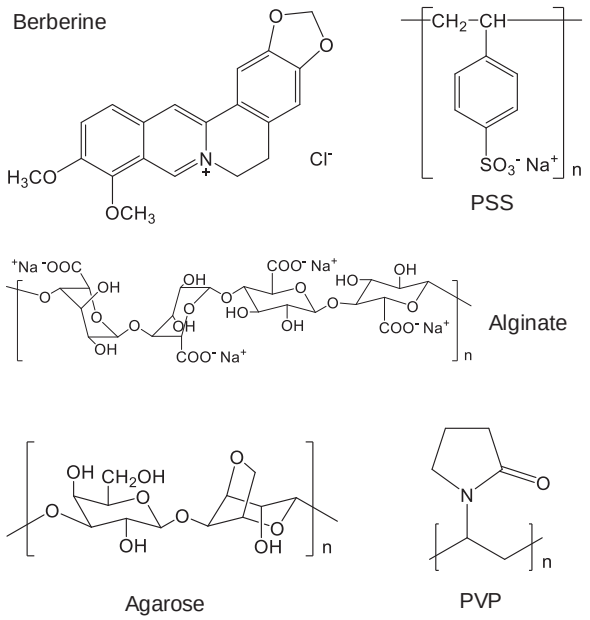

Fig. 1 Structures of berberine and water-soluble polymers, polystyrene sulfonate (PSS), alginate, agarose, and polyvinylpyrrolidone (PVP).

nm. Nanosecond transient absorption measurements were carried out using a homemade system. A third harmonic of a nanosecond Nd: YAG laser (355 nm, 10 Hz, FWHM = 5 ns, Minilite II, Continuum, CA, USA) was employed for the flash photoirradiation. A 500 W xenon arc lamp (Xenon short arc lamp ballast, USHIO Inc., Tokyo, Japan) was used as the monitor light source. A monochromator (G-250, Nikon, Tokyo, Japan) was used to select the wavelength of the transmitted monitor light. The output of the light was detected using a photomultiplier tube (R-928, Hamamatsu Photonics K.K.), its power supply (HTV-C665, Hamamatsu Photonics K.K.), and an oscilloscope (TDS-520D, 500 MHz, Tektronix, OR, USA). The $^1O_2$ generation was measured by near-infrared luminescence at around 1,270 nm from $^1O_2$. The excitation wavelength for $^1O_2$ detection was 355 nm. The quantum yield of $^1O_2$ generation (Φ_Δ) was determined by the comparison of near-infrared emission intensity with a reference photosensitizer, methylene blue (Φ_Δ: 0.52) [14].

RESULTS AND DISCUSSION

The fluorescence intensity of berberine in an aqueous solution was very weak (Φ_f: less than 10^{-3} in a 10 mM sodium phosphate buffer (pH 7.6)), due to intramolecular electron transfer, as previously reported [2,10]. Agarose and PVP, water-soluble neutral polymers, could not increase the fluorescence intensity of berberine, suggesting that there is no interaction between berberine and neutral polymers. Sodium alginate, an anionic polymer, slightly increased the relative fluorescence quantum yield of berberine (+3%). DNA strongly increased the fluorescence intensity of berberine through electrostatic interaction and groove binding [2,10]. However, the fluorescence enhancement effect of alginate was very weak. These results suggest that the structure of alginate is not appropriate for effective electrostatic interaction with berberine. PSS, which is also an anionic polymer, effectively enhanced the fluorescence intensity of berberine (Fig. 2A). PSS has been used for treating hyperkalemia [15]. The observed Φ_f of berberine with 100 μM (monomer unit) in a 10 mM sodium phosphate buffer (pH 7.6) was 0.03, whereas that without PSS was less than 10^{-3}. The τ_f value of berberine was also significantly increased through interaction with PSS (Fig. 2B). The monomer unit of PSS is relatively small, and the structure of PSS is relatively flexible. The structural effect of PSS may be appropriate for interaction with berberine. The absorption spectrum of berberine (peak wavelength: 421 nm) was redshifted through the interaction with PSS (peak wavelength: 430 nm; in the presence of 100 μM PSS), similarly to the effect of DNA [10, 16]. The relatively large redshift (9 nm) of the absorption peak of berberine, which is comparable with that of adenine/thymine-rich DNA, suggests that this interaction is through electrostatic force [10]. Another possible interaction, for example, hydrophobic interaction, cannot explain this large redshift [16]. Relevantly, it has been reported that the sulfonate groups of calixarene can interact with N-methylpyridine, a cationic compound, through electrostatic force [17]. These

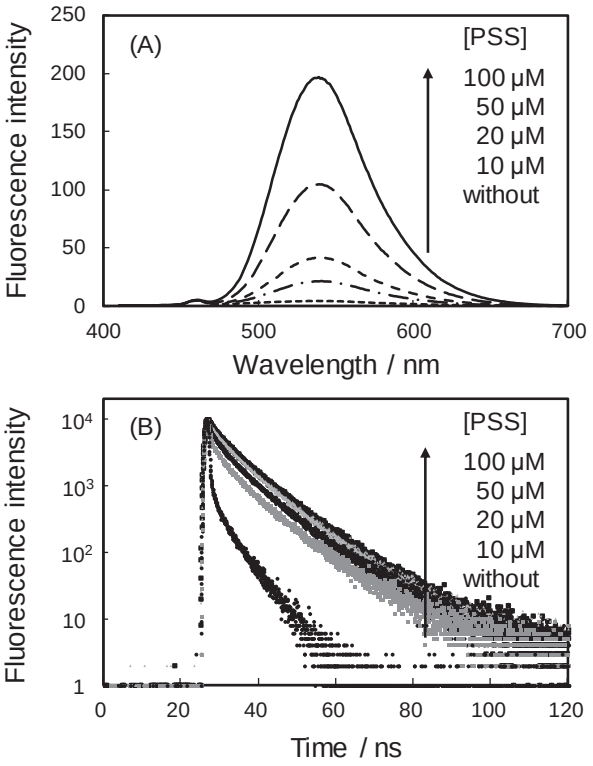

Fig. 2 Fluorescence spectra of berberine with or without PSS (A) and their time profiles (B). The sample solution contained 50 μM berberine and the indicated concentration of PSS in a 10 mM sodium phosphate buffer (pH 7.6). The excitation wavelength for these measurements was 394 nm. The analyzed τ_f values (relative amplitudes) were as follows: 0.11 ns (75%), 1.32 ns (8%), and 5.47 ns (17%) without PSS; and 1.22 ns (7%), 6.68 ns (59%), and 13.0 ns (34%) with 100 μM PSS.

results can be explained by the fact that an electrostatic interaction with PSS suppressed the intramolecular electron transfer-mediated quenching, as in the case of berberine and DNA [10]. The equilibrium of binding interaction between berberine and PSS (1 : *n* complex formation) can be expressed as follows:

$$\text{Berberine} + n\text{PSS(mono)} \rightleftarrows \text{Berberine-PSS(mono)}_n \quad (1),$$

where PSS(mono) is the monomer unit of PSS and Berberine-PSS(mono)$_n$ is the binding complex. The binding constant (K) can be obtained by the following equations:

$$K = \frac{[\text{Berberine}-\text{PSS(mono)}_n]}{[\text{Berberine}][\text{PSS(mono)}]^n} \quad (2),$$

and

$$Log\,\frac{F_0-F}{F} = Log\,K + n Log[\text{PSS(mono)}] \quad (3),$$

where [Berberine-PSS(mono)$_n$], [Berberine], and [PSS(mono)] are the concentrations of berberine-PSS complex, non-binding berberine, and PSS monomer unit, respectively, F_0 is the fluorescence intensity of berberine without PSS, and F is that with PSS. The estimated value of n was about two, suggesting the formation of almost a 1:2 complex of berberine and PSS monomer units. The molecular mechanics calculation supports the conclusion that two PSS units interact with one berberine molecule (Fig. 3). The K value (3.1×10^7 M^{-1}) suggests the formation of a relatively stable complex. The thermodynamic parameters of this complexation at a standard state (298 K, 1 atm), which were calculated from the temperature dependence of K values by the van't Hoff equation, were as follows: enthalpy change (ΔH^o: -250 kJ mol^{-1}), entropy change (ΔS^o: -0.77 kJ mol^{-1} K^{-1}), and Gibbs energy (ΔG^o: -18 kJ mol^{-1}). The negative ΔH^o indicates that the binding interaction is enthalpy driven. The relatively large enthalpy change also supports the electrostatic interaction. The negative ΔS^o suggests that berberine is regularly arranging along the PSS chain.

The observed absorbance of the transient absorption spectrum around 500~600 nm of 50 μM berberine with 100 μM PSS, assigned to the triplet excited (T_1) state of berberine [3], was about twice as large as that without PSS. It is considered that the fluorescence enhancement of berberine through interaction with PSS affects the transient absorption at around this wavelength region. Fluorescence emission apparently decreases the signal of transient absorption. Therefore, the actual transient absorbance of berberine with PSS is considered to be larger than the observed signal. This result suggests the enhancement of intersystem crossing to the T_1 state. Photosensitized $^1O_2$ generation by berberine was also enhanced by PSS (Φ_Δ: 0.5% with 100 μM PSS and 0.08% without PSS).

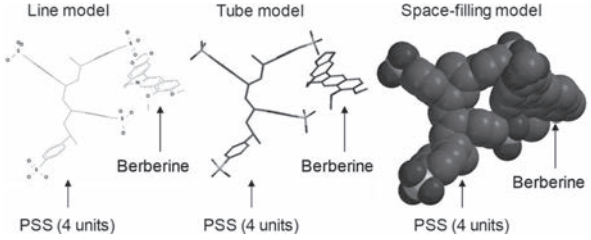

Fig. 3 The optimized structure of the berberine-PSS complex. The structure of berberine and four units of PSS were optimized by a molecular mechanics calculation utilizing Spartan 18' (Wavefunction Inc., CA, USA).

CONCLUSIONS

The S_1 state of berberine in an aqueous solution rapidly relaxes to the ground state through intramolecular electron transfer [10]. Electrostatic interaction with PSS raises the energy level of the intramolecular electron transfer state, similarly to the case of DNA (Fig. 4). This interaction suppresses the self-quenching of the berberine photoexcited state to improve the photosensitizing activity of berberine. Berberine itself is used as a medicinal compound [8,9], and PSS is also used as an agent for treating hyperkalemia [15]. The combination of berberine and PSS may have applications for photomedicinal purposes, such as PDT and photo-sterilization.

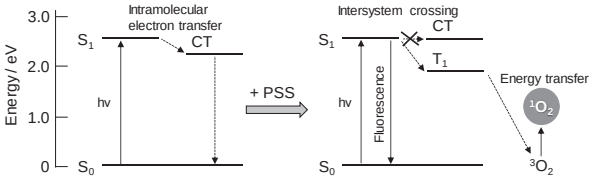

Fig. 4 Scheme of the process of relaxing photoexcited berberine with and without PSS. CT: Charge-transfer state.

Acknowledgments

This work was supported in part by Grant-in-Aid for Scientific Research (B) from Japanese Society for the Promotion of Science (JSPS KAKENHI 17H03086).

Notes

The authors declare no conflict of interests.

References

1. Mansoori B, Mohammadi A, Amin Doustvandi M, Mohammadnejad F, Kamari F, Gjerstorff MF, Baradaran B, Hamblin MR. Photodynamic therapy for cancer: Role of natural products. Photodiagnosis Photodyn Ther, 2019;26:395–404.
2. Hirakawa K, Kawanishi S, Hirano T. The mechanism of guanine specific photooxidation in the presence of berberine and palmatine: activation of photosensitized singlet oxygen generation through DNA-binding interaction. Chem Res Toxicol, 2005;18:1545−1552.
3. Hirakawa K, Kitagawa A, Okazaki S, Ema F, Kobori Y. Photosensitizing activity of berberine-

cyclodextrin inclusion complexes. Photomedicine and Photobiology, 2019;40:7–10.
4. Dolmans DEJGJ, Fukumura D, Jain RK. Photodynamic therapy for cancer. Nat Rev Cancer, 2003;3:380–387.
5. Kessel D. Photodynamic therapy: A brief history. J Clin Med, 2019;8:1581.
6. Ghorbani J, Rahban D, Aghamiri S, Teymouri A, Bahador A. Photosensitizers in antibacterial photodynamic therapy: an overview. Laser Ther, 2018;27:293–302.
7. Weber HA, Zart MK, Hodges AE, Molloy HM, O'Brien BM, Moody LA, Clark AP, Harris RK, Overstreet JD, Smith CS. Chemical comparison of Goldenseal (*Hydrastis canadensis* L.) root powder from three commercial suppliers. J Agric Food Chem, 2003;51:7352–7358.
8. Neag MA, Mocan A, Echeverría J, Pop RM, Bocsan CI, Crişan G, Buzoianu AD. Berberine: botanical occurrence, traditional uses, extraction methods, and relevance in cardiovascular, metabolic, hepatic, and renal disorders. Front Pharmacol, 2018;21:557.
9. Chen CY, Kao CL, Liu CM. The cancer prevention, anti-inflammatory and anti-oxidation of bioactive phytochemicals targeting the TLR4 signaling pathway. Int J Mol Sci, 2018;19:2729.
10. Hirakawa K, Hirano T, Nishimura Y, Arai T, Nosaka Y. Dynamics of singlet oxygen generation by DNA-binding photosensitizers. J Phys Chem B, 2012;116:3037–3044.
11. Inbaraj JJ, Kukielczak BM, Bilski P, Sandvik SL, Chignell CF. Photochemistry and photocytotoxicity of alkaloids from Goldenseal (*Hydrastis canadensis* L.) 1. Berberine. Chem Res Toxicol, 2001;14:1529–1534.
12. Yang Y, Yang HF, Liu YL, Liu ZM, Shen GL, Yu RQ. Cetyltrimethylammonium assay using fluorescence probe berberine and a competitive host–guest complexation with butylated *β*-cyclodextrin. Sensors Actuators B, 2005;106:632−640.
13. Jia B, Li Y, Wang D, Duan R. Study on the interaction of β-cyclodextrin and berberine hydrochloride and its analytical application. PLoS One, 2014;9:e95498.
14. Usui Y, Kamogawa K. A standard system to determine the quantum yield of singlet oxygen formation in aqueous solution. Photochem Photobiol, 1974;19:245–247.
15. Beccari MV, Meaney CJ. Clinical utility of patiromer, sodium zirconium cyclosilicate, and sodium polystyrene sulfonate for the treatment of hyperkalemia: an evidence-based review. Core Evid, 2017;12:11–24.
16. Hirakawa K, Hirano T. The microenvironment of DNA switches the activity of singlet oxygen generation photosensitized by berberine and palmatine. Photochem Photobiol, 2008;84:202–208.
17. Lang K, Mosinger J, Wagnerová DM. Photophysical properties of porphyrinoid sensitizers non-covalently bound to host molecules; models for photodynamic therapy. Coordination Chem Rev, 2004;248:321–350.